ADVANCED MATERIALS TECHNOLOGIES
www.advmattechnol.de

Self-Powered All-Optical Tactile Sensing Platform for User-Interactive Interface

Ruilai Wei, Jiaqi He, Shuaipeng Ge, Hu Liu, Xiaole Ma, Juan Tao, Xi Cui, Xiaoming Mo, Zhou Li, Chunfeng Wang, and Caofeng Pan**

User-interactive interfaces, converting tactile stimuli into readable signals to users and devices simultaneously, improve the communication and interaction between human and machines and therefore greatly contribute to the safety and dexterity during the interactions. However, the concomitant challenges of current user-interactive interfaces such as complex architecture, massive electrodes and fussy cable connections, bulky and unhandy power supply, and deficiency in multistimuli responses have yet to be solved. Herein, an all-optical tactile sensing platform consisting of heterogeneous mechanoluminescent materials and polymer matrix is proposed for the conversion of multiple tactile stimuli into heterochromatic lights in an untethered and self-powered manner. The all-optical tactile sensing platform can respond to tiny shear force such as fingertip slipping with a low limit of 2 N and wide range of strains ranging from 30% to 70% with appropriate discrimination. Most importantly, the visualization of tactile stimuli with human- and machine-readability and vividness permit remote and wireless user-interactive applications such as videogames and RC car control, assisted with the developed method of active optical signal recognition. This work presents a paradigm shift to user-interactive interfaces, boosting their implementation in multitudinous areas such as artificial intelligences and the Internet of Things.

1. Introduction

The rise of virtual/augmented reality and intelligent robots has ignited huge enthusiasms into soft human-machine interface (sHMI), enabling the intuitive cognition and interaction between users and devices without sacrificing motion freedom and comfortability.[1–3] Electronic skin with biomimetic tactile sensing represents one of the most promising schemes to such sHMI, owning to its mechanical compliance, physical imperception, and multifunction.[4–8] Thus, emerging materials such as nanowires/fibers,[9–12] nanomembranes,[13,14] conductive polymers,[15–17] organohydrogels,[18–20] liquid metals,[21] and MXenes,[22–26] combined with novel constructions including mesh,[27,28] serpentine,[29] textile,[30–33] wrinkle,[23] and micropattern,[34–36] assisted with the emerging fabrication methods such as 3D printing,[37] 4D printing,[38] and transfer printing,[39] have been developed for contact/noncontact interactive electronic skin, on the basis of different mechanisms of piezoresistive,[27] capacitive,[40] piezoelectric,[41] and triboelectric.[42–45] Despite the thriving progress, the lack of human-readable output from these interactive interfaces defers the adjustment and adaptability of human operations, imposing restriction on their further widespread applications. Light with transformational color, intensity, or propagation upon tactile stimuli promises a solution to this end because of its readability and intuitiveness. Accordingly, user-interactive interfaces converting tactile stimuli into optical signals that are simultaneously recognizable to users and devices have been proposed, enabled by the integration of pressure sensing elements with electroluminescent/electrochromic devices,[46–49] or by the fabrication of nanowire light-emitting

R. Wei, X. Ma, X. Mo, C. Pan
Center on Nanoenergy Research
School of Physical Science and Technology
Guangxi University
Nanning, Guangxi 530004, P. R. China
E-mail: cfpan@binn.cas.cn

R. Wei, J. He, S. Ge, J. Tao, X. Cui, Z. Li, C. Wang, C. Pan
CAS Center for Excellence in Nanoscience
Beijing Key Laboratory of Micro-nano Energy and Sensor
Beijing Institute of Nanoenergy and Nanosystems
Chinese Academy of Sciences
Beijing 100083, P. R. China

The ORCID identification number(s) for the author(s) of this article can be found under https://doi.org/10.1002/admt.202200757.

DOI: 10.1002/admt.202200757

J. He, X. Cui, Z. Li, C. Pan
School of Nanoscience and Technology
University of Chinese Academy of Sciences
Beijing 100049, P. R. China

S. Ge, J. Tao, C. Wang, C. Pan
Key Laboratory of Optoelectronic Devices and Systems of Ministry of Education and Guangdong Province
College of Physics and Optoelectronic Engineering
Shenzhen University
Shenzhen 518060, P. R. China
E-mail: cfwang@szu.edu.cn

H. Liu
National Engineering Research Center for Advanced Polymer Processing Technology
Zhengzhou University
Zhengzhou 450002, P. R. China

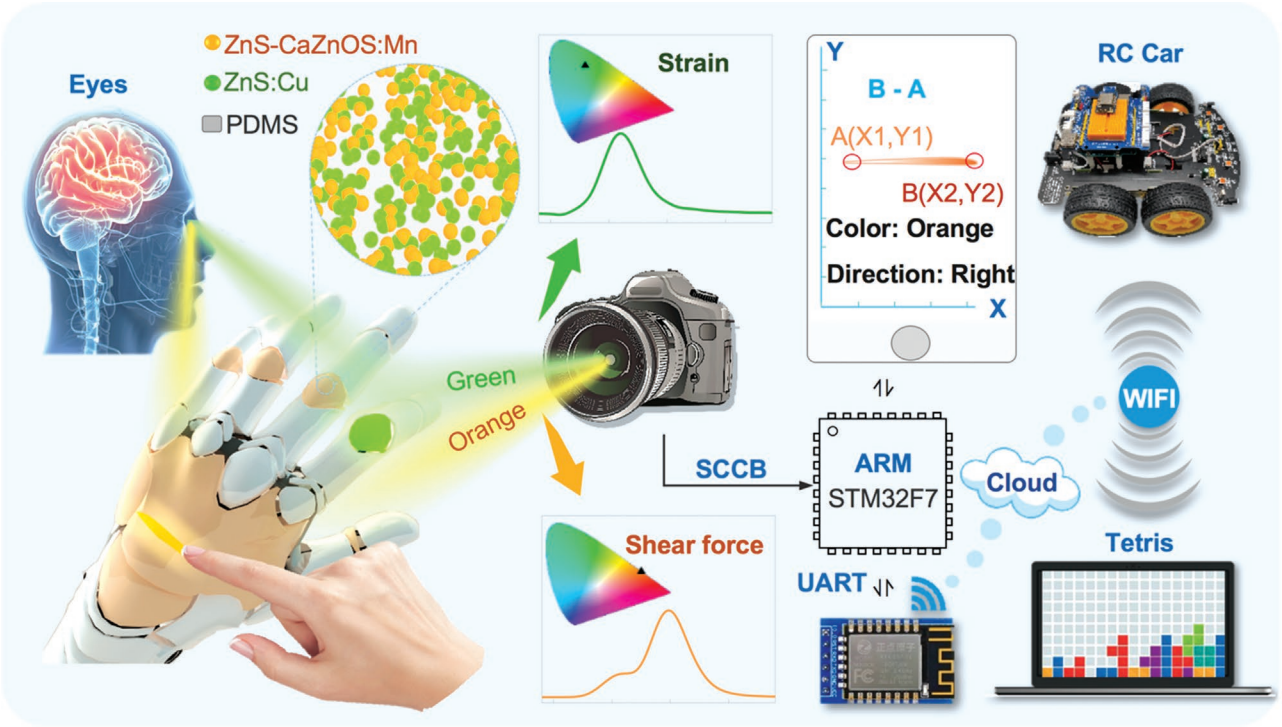

Figure 1. Scheme of the proposed all-optical tactile sensing platform (ATSP) for user-interactive interfaces. The ATSP consists of heterogeneous mechanoluminescent materials and permits the transduction of tactile stimuli into heterochromatic lights that are simultaneously recognizable to users and devices, endowing the remote and dexterous manipulations of user-interactive devices in an untethered, self-powered, and adaptive manner.

diode array with piezo-phototronic effect,[50,51] or by the development of metasurfaces with reversible structural colors,[52] or by the electro-optic conversion via the Pockels effect,[53] or by the conjunction of microcracked shutters and fluorescent materials,[54,55] or by the utilization of self-luminescent materials with piezo/tribophotonic effect,[56–58] or by the synthesis of novel electrochemiluminescence materials with piezo-ionic effect.[59] However, the aforementioned devices suffer from one or more disadvantages of complex architecture, massive electrodes and cables, power supply, and inability of multistimuli responses, and have barely been explored for user-interactive applications due to the lack of an appropriate approach for the recognition of active optical signals.

Herein, an all-optical tactile sensing platform (ATSP) with attributes of minimalist construction, electrode/cable-free, energy autonomy, and multistimuli responses is proposed for user-interactive applications, assisted with the developed strategy for active optical signal recognition. As displayed in **Figure 1**, this ATSP is composed of heterogeneous mechanoluminescent (ML) materials of copper-doped zinc sulfide (ZnS:Cu) and manganese-doped oxysulfide (ZnS-CaZnOS:Mn) embedded in polydimethylsiloxane (PDMS) matrix, permitting the transduction of strain and shear force into heterochromatic lights of green and orange, respectively, in an unambiguous way. The ATSP can respond to tiny shear force such as fingertip slipping with a low limit of 2 N and wide range of strains ranging from 30% to 70%. The visualization of tactile stimuli not only endows information with vividness and human-readability, and therefore much better human-machine interaction through adaptions, but also allows for the wireless capture of signals via an optical instrument, and then expediently differentiated and coded with the developed program to deliver the determined instructions for remote and dexterous manipulations of videogames and RC car in real-time. Along with the merits of low cost on fabrication and ease of scale up, this presented ATSP holds great promise to broad application scenarios such as virtual/augmented reality and intelligent robots.

2. Results and Discussion

2.1. Heterogeneous ML Materials for ATSP

The unique mechano-optical response feature of ML materials without requiring any auxiliary circuit and power supply make them prime candidates for tactile sensing. In our case, two high-performance ML materials of ZnS-CaZnOS:Mn and ZnS:Cu were selected and embedded into PDMS matrix to construct this ATSP, bestowing the transduction of shear force and strain into heterochromatic lights with discrepant and vivid colors, as well as high brightness, as depicted in **Figure 2**a and Video S1, Supporting Information. The distinctive response of ZnS-CaZnOS:Mn and ZnS:Cu to shear force and strain is determined by the dominant ML mechanism of piezophotonic and tribophotonic, respectively.[60,61] Upper-right inset of Figure 2a shows the false-color SEM image of the ATSP. The ZnS-CaZnOS:Mn was synthesized via the conventional high-temperature solid state reaction method (see Section 4 for details). The ZnS-CaZnOS:Mn is a biphase hybrid consisting of ZnS phase and CaZnOS phase, as determined by the

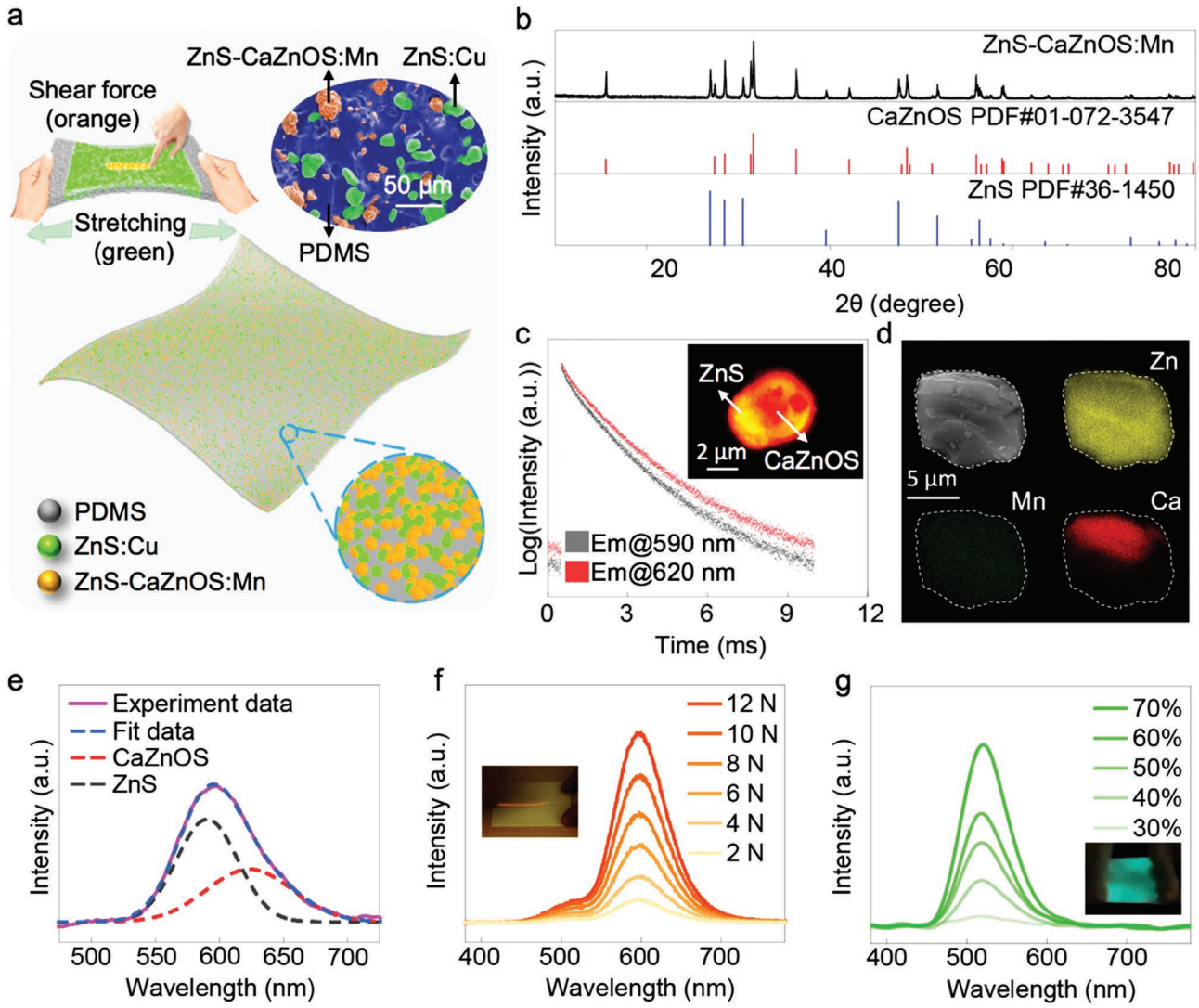

Figure 2. Heterogeneous ML Materials for ATSP. a) Schematic of the ATSP composed of heterogeneous mechanoluminescent materials of ZnS:Cu and ZnS-CaZnOS:Mn and PDMS matrix, permitting the transduction of strain and shear force into heterochromatic lights of green and orange (upper-left inset), respectively. Upper-right inset: the false-color SEM image of ZnS:Cu and ZnS-CaZnOS:Mn particles embedded into PDMS matrix. b) XRD pattern of the ZnS-CaZnOS:Mn. c) The transient photoluminescence decay curves of ZnS-CaZnOS:Mn. Inset shows the fluorescence microscope image of one representative ZnS-CaZnOS:Mn particle. d) The EDS mapping images of one representative ZnS-CaZnOS:Mn particle. e) The deconvolution of a representative ML spectrum of ZnS-CaZnOS:Mn. f) The ML spectra of ATSP under different shear forces. Inset shows the light-emitting photograph of ATSP upon fingertip slipping. g) The ML spectra of ATSP upon variable strain at a stretch-release frequency of 3 Hz. Inset shows the light-emitting photograph of ATSP upon stretching.

X-ray diffraction (XRD) pattern (Figure 2b), whose diffraction peaks match well with either standard ZnS (PDF #36-1450) or standard CaZnOS (PDF #01-072-3547). The biphase feature can be further confirmed by the fluorescence microscope image and energy-dispersive X-ray spectroscopy (EDS) mapping images of a representative ZnS-CaZnOS:Mn particle. Two distinct emission colors can be observed in the fluorescence microscope image of one single ZnS-CaZnOS:Mn particle (inset of Figure 2c), attributing to photoluminescent emission of ZnS:Mn and CaZnOS:Mn, respectively. This result is consistent with the transient photoluminescence decay curves that exhibits two different delay lifetimes upon excitation at 290 nm with the monitored wavelength of 590 nm (ZnS:Mn) and 620 nm (CaZnOS:Mn), as shown in Figure 2c. The separation of Ca and Zn element occurs within one single ZnS-CaZnOS:Mn particle due to its biphase nature (Figure 2d), while Mn element uniformly distribute in the whole particle, suggesting the successful doping of Mn into ZnS and CaZnOS simultaneously, both of which contribute to the final ML emission, as identified by the deconvolution of a representative ML spectrum (Figure 2e). The phase heterojunction between ZnS and CaZnOS can give rise to the energy band offset, which boosts the carrier transfer and recombination therein to enhance the ML performance.[62] In conjunction with the commercial ZnS:Cu, the ATSP was constructed (see Section 4 for fabrication details). The ATSP can respond to tiny shear forces such as

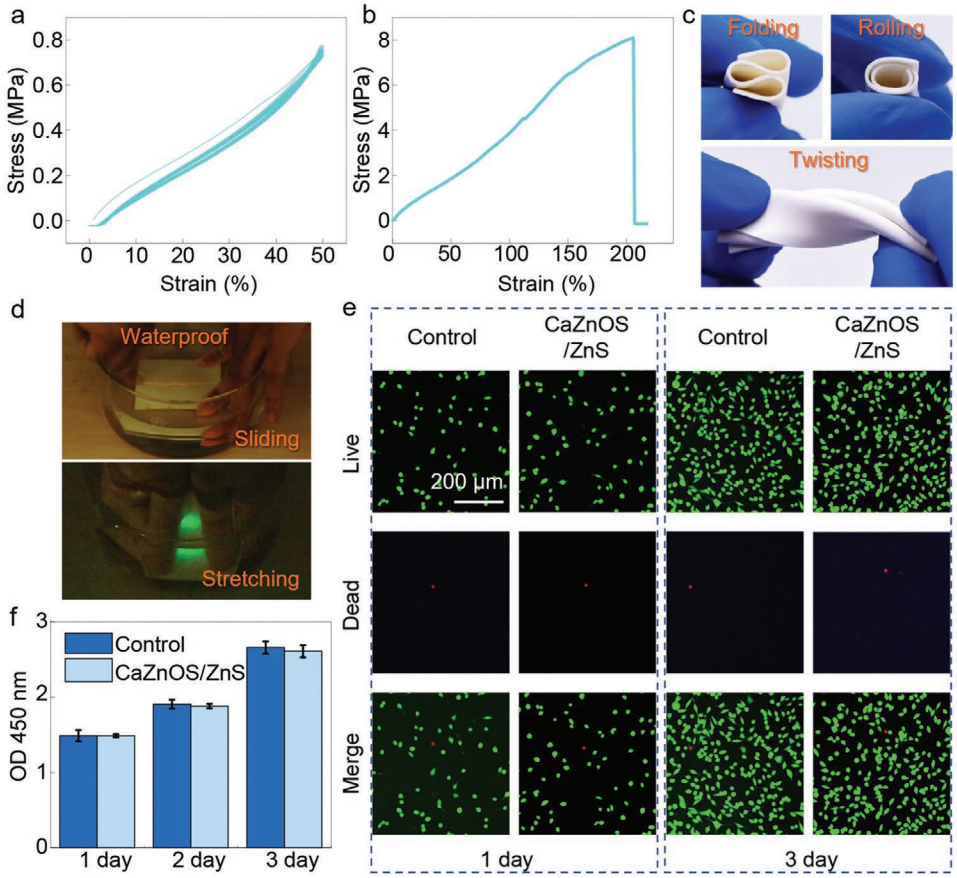

Figure 3. Characterizations of ATSP. a) The cyclic stress-strain test of ATSP with a maximal strain of 50%, showing no obviously mechanical attenuation after 100 loading-unloading cycles. b) The stress–strain curve of ATSP with a fracture strain of 205%. c) Optical images of ATSP upon folding, rolling and twisting, showing its mechanical robustness. d) Under-water illuminations of ATSP, showing its waterproof ability. e) Fluorescence images of L929 cells after culturing on ATSP and control sample for different days, respectively, in which the live cells were stained green and the dead cells were stained red. f) The cell proliferation of L929 cells determined by CCK-8 assay (five samples were tested for each time interval).

fingertip slipping (inset of Figure 2f), with an intensive orange illumination at peak wavelength of 600 nm, and the peak position did not shift as the force increased from 2 to 12 N, as shown in Figure 2f. Simultaneously, the ATSP can emit green light with consistent peak wavelength of 520 nm under variable strains from 30% to 70%, permitting the visualization of strain sensing (Figure 2g and inset). More importantly, the ATSP manifests a distinguishable light-emission upon the simultaneously applied strain and shear force, as proved by the ML spectrum with two identified peaks in Figure S1, Supporting Information and Video S2, Supporting Information. The differentiated and interference-free light-emissions upon shear force and strain prove the ability of ATSP to decouple tactile stimuli, ensuring the expedient identification of human operation intents.

Meanwhile, the ATSP exhibits excellent mechanical properties, with an elastic strain of 50% that is qualified to wearable applications (**Figure 3**a), and a fracture strain of over 200% (Figure 3b), ensuring the large and reversible deformations such as folding, rolling, and twisting with robustness (Figure 3c). In addition, the ATSP is waterproof without any additional packaging, benefitting from the encapsulation of ML materials into PDMS, thereby holding great potential for under-water applications (Figure 3d). More importantly, the cytotoxicity testing indicates the good biosafety and biocompatibility of the ATSP, where the viabilities of L929 cells between the experimental group and blank group did not show any significant difference after 3 days of culture, as confirmed by the confocal microscope images with immunofluorescent staining of live (green) and dead (red) cells (Figure 3e and Figure S2, Supporting Information), as well as the cell proliferation determined by Cell Count Kit-8 (CCK-8) assay (Figure 3f, see Section 4 for details).

2.2. Active Optical Signal Recognition for Logic Instructions

To realize the user-interactive applications, an architecture that is able of encoding the active ML signals into machine-readable logic instructions is developed. As displayed in **Figure 4**a, the architecture comprises three units: i) ML signals generation upon tactile stimuli; ii) programs burned into microcontroller unit (MCU) to enable ML signals recognition; iii) ML signals processing and encoding along with instructions transmission. And color discrimination and trajectory recognition of ML signals are among two significant steps for successful

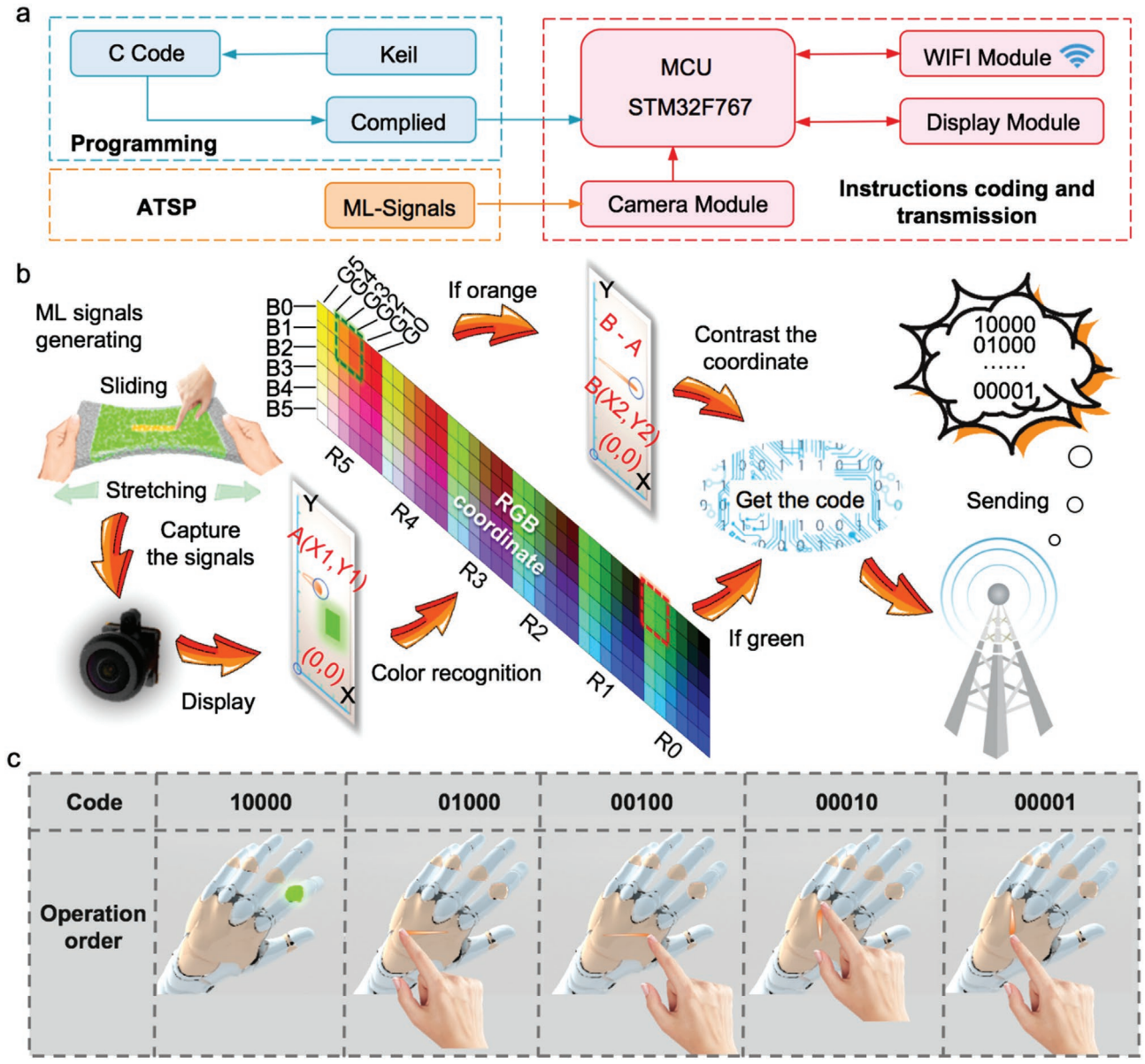

Figure 4. Active optical signal recognition method for logic instructions. a) Flowchart of the active optical signal recognition method. b) Illustrated process of color discrimination and optical trajectory orientation recognition of ML signals. c) The logic instructions with corresponding codes determined by the active optical signal recognition method.

implementation. As elaborated in Figure 4b, the visual ML signals with tactile information are firstly captured by an optical receiver (OV5640 camera), and then recognized by the program embedded in MCU (STM32F767), and dynamically displayed on an LCD screen with each pixel corresponding to a set of RGB component in a color coordinate system and synchronously a spatial position in a Cartesian coordinate system. In the case of color discrimination, the obtained RGB components are compared to the preselected ones, as indicated by rectangle dotted areas in the color coordinate system with values of (R,G,B) = (0,5,0), (0,5,1), (0,4,0), and (0,4,1) for green light, and (R,G,B) = (5,3,0), (5,3,1), (5,2,0), and (5,2,1) for orange light, respectively. The optimized amount of preselected RGB components ensures the accuracy of color recognition as well as certain error-tolerance ability. The green ML signals are directly assigned to operation commands of on/off switching with a binary code of "10000", while the orange ML signals are processed further to identify the motion trajectory orientations for multidimensional manipulation. A Cartesian coordinate system is established on the LCD screen with the lower-left pixel as the origin of (X_0,Y_0) = (0,0), in which the motion orientations of orange ML signals can be determined by comparing the spatial coordinates of (X_1,Y_1) and (X_2,Y_2) recorded by the camera from starting frame to the ending frame, and then motions with orientations parallel to coordinate axis (see Figure S3, Supporting Information and Note S1, Supporting Information for parallel identification) are selected and codified into binary codes of "01000", "00100", "00010", and "00001" via MCU for device control. The

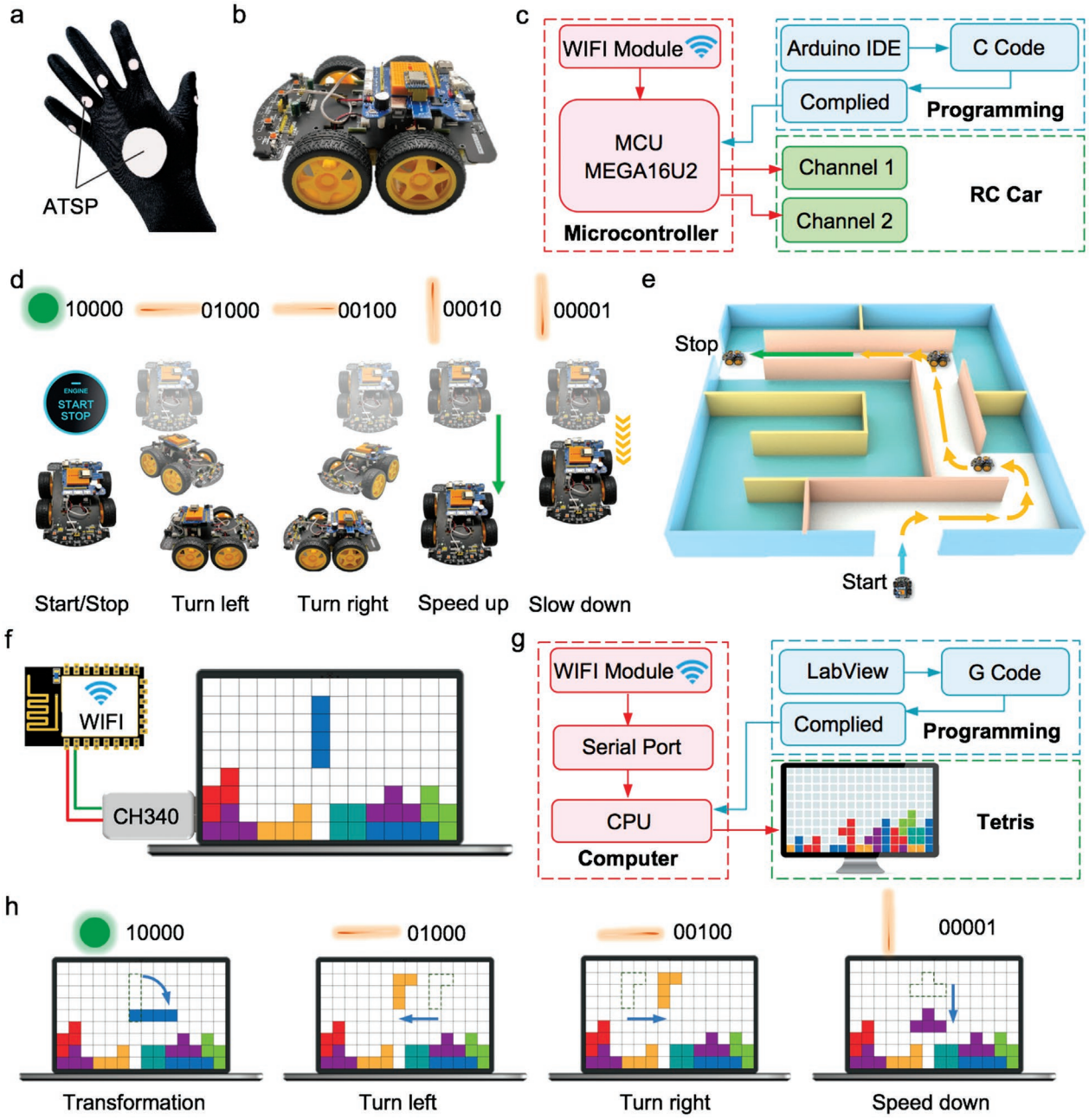

Figure 5. ATSP for user-interactive applications. a) An optical tactile sensing glove with assembled ATSP on dorsum and joints for all-optical operation. b) Photo of RC car that is configured for the demo of optical tactile sensing glove. c) Flowchart of RC car operation with units of instructions reception, recognition, and implementation. d) The logic instructions and the corresponding actions of RC car. e) Optical tactile sensing glove for RC car maze-through operation with great operability due to the eye-hand cooperation for adaptation. f) Optical tactile sensing glove for computer control with the WIFI module connected to computer using a USB bus of CH340. g) The block diagram of the Tetris game implementation. h) The logic instructions and the corresponding actions during Tetris operation.

logic instructions with corresponding codes are summarized in Figure 4c, which are ready to be uploaded to cloud via a WIFI module and subsequently transmitted to the terminal devices for remote manipulations. The photograph of each module hardware of the active optical signal recognition system is shown in Figure S4, Supporting Information, and the detailed program for color discrimination and motion trajectory orientation identification is presented in Note S2, Supporting Information.

2.3. ATSP for User-Interactive Applications

Integration of tactile sensors into gloves represents a promising paradigm for user-interactive interfaces, encompassing the deft and convenient control of terminal devices with the elimination of conspicuous uncomfortableness and invasiveness. As shown in **Figure 5**a, a tactile glove prototype with assembled ATSP on dorsum and joints is demonstrated. The glove fits hand well

and can visually express the operation logics by virtue of heterogeneous ML emissions (Video S3, Supporting Information), each of which represents an individual control instruction for remote manipulations. Figure 5b shows a RC car configured for the representative demo, where the instructions can be wirelessly received by RC car via the WIFI module (ESP8266) and then recognized by the MCU (MEGA16U2) with embedded programs, which adjust the pulse width modulation (PWM) inputs of channel #1 and #2 to individually control the speeds of vehicle wheels on both sides (Figure 5c, see Note S3, Supporting Information for control details), realizing the motion manipulations of RC car including start and stop, turn left, turn right, speed up, and slow down (Figure 5d). Moreover, an accurate operation of RC car to go through a maze is demonstrated (Figure 5e, Video S4, Supporting Information), enabled by the greater operability of the user-interactive interface with eye-hand cooperation. Meanwhile, the tactile glove can be an operation platform for computer control such as videogames, where the WIFI module is connected to computer using a USB bus (CH340) for wireless instruction receptions (Figure 5f). Figure 5g shows the block diagram of a Tetris game implementation, where the received instructions of "10000", "01000", "00100", and "00001" is projected to "transformation", "move left", "move right", and "speed down", respectively, endowing the Tetris manipulation in an initiative and real-time way (Figure 5h, Video S5, Supporting Information).

3. Conclusions

In summary, we present a self-powered, wireless and all-optical tactile sensing platform enabled by heterogeneous ML materials for user-interactive applications. On the basis of the direct mechano-optical conversion of ML materials without any external power source or auxiliary circuit, the visual expression of multiple tactile stimuli into heterochromatic ML lights in a self-powered and untethered way is achieved. The readability of ML signals to both users and devices enables the tactile sensing platform to be preeminent user-interactive interface for diversified interaction applications. In synchrony with the developed active optical signal recognition approach, the nuanced and wireless operations of RC Car and videogames are demonstrated, with great agility and adaptability because of the enabled eye-hand cooperation by the user-interactive interface. Moreover, the tactile sensing platform is construction-minimalist, free of electrodes and cables, ease of scale up, cost-efficient, mechanically compliant and robust, and biocompatible, thereby holding great potential in an incredible number of applications such as virtual/augmented reality, intelligent robots and the Internet of Things.

4. Experimental Section

Synthesis of ML Materials: The ZnS-CaZnOS:Mn was synthesized via the high-temperature solid state reaction method, as reported by our previous publication.[60] Briefly, the raw materials including eggshell powder with an estimated $CaCO_3$ content of 90 wt%, ZnS power (99.99% metals basis, 3.3–4.3 µm, Aladdin), and $MnCO_3$ (≥99.9% trace metals basis, Sigma Aldrich) powder were adequately mixed in a ball mill at 450 r min^{-1} for 30 min with a molar ratio of Ca:Zn:Mn = 1:2:0.01. The obtained mixtures were transferred to the horizontal tube furnace and sintered at 1100 °C for 4–6 h under the protection of argon gas with a rate of 80 sccm. The products were naturally cooled to room temperature and ground into fine powder for use. The ZnS-CaZnOS:Mn has a mean size of 5.3 µm, as determined by the SEM image in Figure S5a, Supporting Information. The ZnS:Cu was obtained from Shanghai Keyan Phosphor Technology Co.,Ltd, and for utilization as received, which has a mean size of 19.3 µm (Figure S5b, Supporting Information).

Fabrication and Characterizations of ATSP: The ATSP was fabricated by simply mixing ML materials of ZnS:Cu and ZnS-CaZnOS:Mn with the PDMS matrix (Sylgard 184, Dow Corning), followed by the molding at an acrylic mold with a desiccation at 80 °C for overnight in oven. The weight ratio of ML materials to PDMS was 1:1, in which the weight ratio of ZnS:Cu to ZnS-CaZnOS:Mn was 2:3, and the weight ratio of base resin to curing agent of PDMS was 6:1. The thickness of ATSP was around 600 µm. The ML spectra of ATSP upon strains and shear forces were measured via the home-built apparatus consisting of fiber optic spectrometer (QE65 Pro), dynamometer, linear motor, and 3D displacement platform, as shown in Figure S6, Supporting Information. The mechanical performances of ATSP were characterized using the peel strength tester (YL-S70) with a stretching rate of 50 mm min^{-1}.

In Vitro Cellular Viability Test (Cell Count Kit-8, CCK-8): *Cell Culture*: The L929 cell line was cultured in a 25 cm^2 flask containing standard Dulbecco's modified Eagle's medium (DMEM, Gibco) with 1% penicillin/streptomycin (Gibco) and 10% fetal bovine serum (FBS, Gibco), at a culture temperature of 37 °C and a CO_2 atmosphere of 5%.

CCK-8 Assay: The sample of ATSP consisting of 100 mg of mechanoluminescence materials was immersed in 50 mL DMEM for 24 h to obtain the leach liquor. The L929 cells at the Log phase of growth with an initial density of 1×10^6 cell per well were planted into the disposable plate with naked 24 wells, each of which contained 1 mL of leach liquor. And wells with 1 mL of standard DMEM were set as the control group. The cells were cultured for 1, 2, and 3 days, and the cell proliferation level were evaluated by Cell Count Kit-8 (CCK-8, Dojindo Molecular Technologies, Inc., Japan). The samples of experimental and control groups were washed using the phosphate-buffered saline solution (PBS) after removing the culture mediums, followed by the addition of 210 µL complete medium containing 10 µL of CCK-8 reagent. After further incubation for 2 h, 150 µL culture supernatant of the samples were reserved and transferred into a 96-well plate for the absorbance measurement at a wavelength of 450 nm, where each group has five parallel wells.

Cell Morphologic Immunofluorescent Staining: To further confirm the cytocompatibility of the ATSP, live/dead cell staining was used to visibly investigate the cells viability. The cells were washed with PBS for three times, and then stained with Calcein-AM/PI for 20 min at room temperature. The stained cells were visualized by laser scanning confocal microscope (Leica SP8), where the live cells were stained into green, and the dead cells were stained into red.

Statistical Analysis: The deconvolution of a representative ML spectrum of ZnS-CaZnOS:Mn was conducted via Origin software with the fitting function of $y = y_0 + (A/(w\times\sqrt{p_i/2}))\times\exp(-2\times((x-x_c)/w)^2)$. The cell proliferation of L929 cells was determined by CCK-8 assay, in which the data were obtained via the native software (Microplate Manager Software) of the instrument (BIORAD iMark Microplate Reader). Five samples were tested for each time interval and the mean value and the standard deviation were calculated and shown as mean ± standard error.

Supporting Information

Supporting Information is available from the Wiley Online Library or from the author.

Acknowledgements

R.W. and J.H. contributed equally to this work. The authors are thankful for the support from the National Natural Science Foundation of China (52125205, U20A20166, 61805015, 52002246, 61875136, and 61804011), the Shenzhen Fundamental Research Project (JCYJ20190808170601664), the Shenzhen Science and Technology Program (KQTD20170810105439418), the Science and Technology Innovation Project of Shenzhen Excellent Talents (RCBS20200714114919006), the Fundamental Research Project of Guangdong Province (2020A1515011315), National key R&D program of China (2021YFB3200304), and the Fundamental Research Funds for the Central Universities.

Conflict of Interest

The authors declare no conflict of interest.

Data Availability Statement

The data that support the findings of this study are available from the corresponding author upon reasonable request.

Keywords

artificial skin, intelligent robots, mechanoluminescence, user-interactive interface, visual tactile sensing

Received: May 8, 2022
Revised: June 18, 2022
Published online:

[1] X. Yu, Z. Xie, Y. Yu, J. Lee, A. Vazquez-Guardado, H. Luan, J. Ruban, X. Ning, A. Akhtar, D. Li, B. Ji, Y. Liu, R. Sun, J. Cao, Q. Huo, Y. Zhong, C. Lee, S. Kim, P. Gutruf, C. Zhang, Y. Xue, Q. Guo, A. Chempakasseril, P. Tian, W. Lu, J. Jeong, Y. Yu, J. Cornman, C. Tan, B. Kim, et al., *Nature* **2019**, *575*, 473.
[2] T. Reid, J. Gibert, *Science* **2022**, *375*, 149.
[3] Y. Chen, Z. Gao, F. Zhang, Z. Wen, X. Sun, *Exploration* **2022**, *2*, 20210112.
[4] Y. Liu, C. Yiu, Z. Song, Y. Huang, K. Yao, T. Wong, J. Zhou, L. Zhao, X. Huang, S. K. Nejad, M. Wu, D. Li, J. He, X. Guo, J. Yu, X. Feng, Z. Xie, X. Yu, *Sci. Adv.* **2022**, *8*, eabl6700.
[5] S. Pyo, J. Lee, K. Bae, S. Sim, J. Kim, *Adv. Mater.* **2021**, *33*, 2005902.
[6] Q. Shi, B. Dong, T. He, Z. Sun, J. Zhu, Z. Zhang, C. Lee, *InfoMat* **2020**, *2*, 1131.
[7] Z. Lin, G. Zhang, X. Xiao, C. Au, Y. Zhou, C. Sun, Z. Zhou, R. Yan, E. Fan, S. Si, L. Weng, S. Mathur, J. Yang, J. Chen, *Adv. Funct. Mater.* **2022**, *32*, 2109430.
[8] X. Xiao, Y. Fang, X. Xiao, J. Xu, J. Chen, *ACS Nano* **2021**, *15*, 18633.
[9] K. Wang, L. W. Yap, S. Gong, R. Wang, S. J. Wang, W. Cheng, *Adv. Funct. Mater.* **2021**, *31*, 2008347.
[10] T. An, D. V. Anaya, S. Gong, L. W. Yap, F. Lin, R. Wang, M. R. Yuce, W. Cheng, *Nano Energy* **2020**, *77*, 105295.
[11] J. Xiong, J. Chen, P. S. Lee, *Adv. Mater.* **2021**, *33*, 2002640.
[12] X. Wang, Y. Zhang, X. Zhang, Z. Huo, X. Li, M. Que, Z. Peng, H. Wang, C. Pan, *Adv. Mater.* **2018**, *30*, 1706738.
[13] K. Sim, Z. Rao, Z. Zou, F. Ershad, J. Lei, A. Thukral, J. Chen, Q.-A. Huang, J. Xiao, C. Yu, *Sci. Adv.* **2019**, *5*, eaav9653.
[14] Z. Li, W. Ran, Y. Yan, L. Li, Z. Lou, G. Shen, *InfoMat* **2022**, *4*, e12261.
[15] N. Matsuhisa, S. Niu, S. J. K. O'Neill, J. Kang, Y. Ochiai, T. Katsumata, H.-C. Wu, M. Ashizawa, G.-J. N. Wang, D. Zhong, X. Wang, X. Gong, R. Ning, H. Gong, I. You, Y. Zheng, Z. Zhang, J. B. H. Tok, X. Chen, Z. Bao, *Nature* **2021**, *600*, 246.
[16] T. He, Z. Sun, Q. Shi, M. Zhu, D. V. Anaya, M. Xu, T. Chen, M. R. Yuce, A. V.-Y. Thean, C. Lee, *Nano Energy* **2019**, *58*, 641.
[17] P. Tan, H. Wang, F. Xiao, X. Lu, W. Shang, X. Deng, H. Song, Z. Xu, J. Cao, T. Gan, B. Wang, X. Zhou, *Nat. Commun.* **2022**, *13*, 358.
[18] W. Wu, Y. Ren, T. Jiang, L. Hou, J. Zhou, H. Jiang, *Chem. Eng. J.* **2022**, *430*, 132635.
[19] Z. Xu, F. Zhou, H. Yan, G. Gao, H. Li, R. Li, T. Chen, *Nano Energy* **2021**, *90*, 106614.
[20] S. Wan, N. Wu, Y. Ye, S. Li, H. Huang, L. Chen, H. Bi, L. Sun, *Small Struct.* **2021**, *2*, 2100105.
[21] S. Xiang, D. Liu, C. Jiang, W. Zhou, D. Ling, W. Zheng, X. Sun, X. Li, Y. Mao, C. Shan, *Adv. Funct. Mater.* **2021**, *31*, 2100940.
[22] S. Duan, Y. Lin, C. Zhang, Y. Li, D. Zhu, J. Wu, W. Lei, *Nano Energy* **2022**, *91*, 106650.
[23] H. Yang, X. Xiao, Z. Li, K. Li, N. Cheng, S. Li, J. H. Low, L. Jing, X. Fu, S. Achavananthadith, F. Low, Q. Wang, P.-L. Yeh, H. Ren, J. S. Ho, C.-H. Yeow, P.-Y. Chen, *ACS Nano* **2020**, *14*, 11860.
[24] Y. Chen, X. Wei, H. Li, Y. Fan, W. Hu, G. Zhu, *ACS Omega* **2019**, *4*, 20470.
[25] Y. Lu, X. Qu, W. Zhao, Y. Ren, W. Si, W. Wang, Q. Wang, W. Huang, X. Dong, *Research* **2020**, *2020*, 2038560.
[26] H. Liu, X. Chen, Y. Zheng, D. Zhang, Y. Zhao, C. Wang, C. Pan, C. Liu, C. Shen, *Adv. Funct. Mater.* **2021**, *31*, 2008006.
[27] L. Lu, C. Jiang, G. Hu, J. Liu, B. Yang, *Adv. Mater.* **2021**, *33*, 2100218.
[28] Y. Zhang, Z. Huo, X. Wang, X. Han, W. Wu, B. Wan, H. Wang, J. Zhai, J. Tao, C. Pan, Z. L. Wang, *Nat. Commun.* **2020**, *11*, 5629.
[29] Z. Huang, Y. Hao, Y. Li, H. Hu, C. Wang, A. Nomoto, T. Pan, Y. Gu, Y. Chen, T. Zhang, W. Li, Y. Lei, N. Kim, C. Wang, L. Zhang, J. W. Ward, A. Maralani, X. Li, M. F. Durstock, A. Pisano, Y. Lin, S. Xu, *Nat. Electron.* **2018**, *1*, 473.
[30] F. Wen, Z. Zhang, T. He, C. Lee, *Nat. Commun.* **2021**, *12*, 5378.
[31] Y. Luo, Y. Li, P. Sharma, W. Shou, K. Wu, M. Foshey, B. Li, T. Palacios, A. Torralba, W. Matusik, *Nat. Electron.* **2021**, *4*, 193.
[32] G. Chen, X. Xiao, X. Zhao, T. Tat, M. Bick, J. Chen, *Chem. Rev.* **2022**, *122*, 3259.
[33] A. Libanori, G. Chen, X. Zhao, Y. Zhou, J. Chen, *Nat. Electron.* **2022**, *5*, 142.
[34] H. Guo, H. Wang, Z. Xiang, H. Wu, J. Wan, C. Xu, H. Chen, M. Han, H. Zhang, *Adv. Funct. Mater.* **2021**, *31*, 2103075.
[35] Q. He, Y. Wu, Z. Feng, C. Sun, W. Fan, Z. Zhou, K. Meng, E. Fan, J. Yang, *Nano Energy* **2019**, *59*, 689.
[36] P. Zhu, H. Du, X. Hou, P. Lu, L. Wang, J. Huang, N. Bai, Z. Wu, N. X. Fang, C. F. Guo, *Nat. Commun.* **2021**, *12*, 4731.
[37] Z. Zhu, H. S. Park, M. C. McAlpine, *Sci. Adv.* **2020**, *6*, eaba5575.
[38] C.-Y. Liaw, J. Pereyra, A. Abaci, S. Ji, M. Guvendiren, *Adv. Mater. Technol.* **2022**, *7*, 2101118.
[39] Y. Wang, L. Yin, Y. Bai, S. Liu, L. Wang, Y. Zhou, C. Hou, Z. Yang, H. Wu, J. Ma, Y. Shen, P. Deng, S. Zhang, T. Duan, Z. Li, J. Ren, L. Xiao, Z. Yin, N. Lu, Y. Huang, *Sci. Adv.* **2020**, *6*, eabd0996.
[40] W. Zhou, S. Yao, H. Wang, Q. Du, Y. Ma, Y. Zhu, *ACS Nano* **2020**, *14*, 5798.
[41] W. Deng, T. Yang, L. Jin, C. Yan, H. Huang, X. Chu, Z. Wang, D. Xiong, G. Tian, Y. Gao, H. Zhang, W. Yang, *Nano Energy* **2019**, *55*, 516.
[42] H. Wang, J. Wang, K. Yao, J. Fu, X. Xia, R. Zhang, J. Li, G. Xu, L. Wang, J. Yang, J. Lai, Y. Dai, Z. Zhang, A. Li, Y. Zhu, X. Yu, Z. L. Wang, Y. Zi, *Sci. Adv.* **2021**, *7*, eabi6751.
[43] M. Zhu, Z. Sun, Z. Zhang, Q. Shi, T. He, H. Liu, T. Chen, C. Lee, *Sci. Adv.* **2020**, *6*, eaaz8693.
[44] Z. Zhou, K. Chen, X. Li, S. Zhang, Y. Wu, Y. Zhou, K. Meng, C. Sun, Q. He, W. Fan, E. Fan, Z. Lin, X. Tan, W. Deng, J. Yang, J. Chen, *Nat. Electron.* **2020**, *3*, 571.

[45] K. Zhou, Y. Zhao, X. Sun, Z. Yuan, G. Zheng, K. Dai, L. Mi, C. Pan, C. Liu, C. Shen, *Nano Energy* **2020**, *70*, 104546.
[46] C. Wang, D. Hwang, Z. Yu, K. Takei, J. Park, T. Chen, B. Ma, A. Javey, *Nat. Mater.* **2013**, *12*, 899.
[47] C. Larson, B. Peele, S. Li, S. Robinson, M. Totaro, L. Beccai, B. Mazzolai, R. Shepherd, *Science* **2016**, *351*, 1071.
[48] H.-H. Chou, A. Nguyen, A. Chortos, J. W. F. To, C. Lu, J. Mei, T. Kurosawa, W.-G. Bae, J. B. H. Tok, Z. Bao, *Nat. Commun.* **2015**, *6*, 8011.
[49] B. Lee, J.-Y. Oh, H. Cho, C. W. Joo, H. Yoon, S. Jeong, E. Oh, J. Byun, H. Kim, S. Lee, J. Seo, C. W. Park, S. Choi, N.-M. Park, S.-Y. Kang, C.-S. Hwang, S.-D. Ahn, J.-I. Lee, Y. Hong, *Nat. Commun.* **2020**, *11*, 663.
[50] C. Pan, L. Dong, G. Zhu, S. Niu, R. Yu, Q. Yang, Y. Liu, Z. L. Wang, *Nat. Photonics* **2013**, *7*, 752.
[51] R. Bao, J. Tao, C. Pan, Z. L. Wang, *Small Sci.* **2021**, *1*, 2000060.
[52] Y.-J. Quan, Y.-G. Kim, M.-S. Kim, S.-H. Min, S.-H. Ahn, *ACS Nano* **2020**, *14*, 5392.
[53] B. Dong, Y. Yang, Q. Shi, S. Xu, Z. Sun, S. Zhu, Z. Zhang, D.-L. Kwong, G. Zhou, K.-W. Ang, C. Lee, *ACS Nano* **2020**, *14*, 8915.
[54] J. Li, Z. Yuan, X. Han, C. Wang, Z. Huo, Q. Lu, M. Xiong, X. Ma, W. Gao, C. Pan, *Small Sci.* **2021**, *2*, 2100083.
[55] Y. Zhao, W. Gao, K. Dai, S. Wang, Z. Yuan, J. Li, W. Zhai, G. Zheng, C. Pan, C. Liu, C. Shen, *Adv. Mater.* **2021**, *33*, 2102332.
[56] X. Wang, H. Zhang, R. Yu, L. Dong, D. Peng, A. Zhang, Y. Zhang, H. Liu, C. Pan, Z. L. Wang, *Adv. Mater.* **2015**, *27*, 2324.
[57] X. Y. Wei, X. Wang, S. Y. Kuang, L. Su, H. Y. Li, Y. Wang, C. Pan, Z. L. Wang, G. Zhu, *Adv. Mater.* **2016**, *28*, 6656.
[58] X. Zhao, Z. Zhang, Q. Liao, X. Xun, F. Gao, L. Xu, Z. Kang, Y. Zhang, *Sci. Adv.* **2020**, *6*, eaba4294.
[59] J. I. Lee, H. Choi, S. H. Kong, S. Park, D. Park, J. S. Kim, S. H. Kwon, J. Kim, S. H. Choi, S. G. Lee, D. H. Kim, M. S. Kang, *Adv. Mater.* **2021**, *33*, 2100321.
[60] C. Wang, R. Ma, D. Peng, X. Liu, J. Li, B. Jin, A. Shan, Y. Fu, L. Dong, W. Gao, Z. L. Wang, C. Pan, *InfoMat* **2021**, *3*, 1272.
[61] W. Wang, Z. Wang, J. Zhang, J. Zhou, W. Dong, Y. Wang, *Nano Energy* **2022**, *94*, 106920.
[62] D. Peng, Y. Jiang, B. Huang, Y. Du, J. Zhao, X. Zhang, R. Ma, S. Golovynskyi, B. Chen, F. Wang, *Adv. Mater.* **2020**, *32*, 1907747.